Catalysis Science & Technology

Accepted Manuscript

ROYAL SOCIETY OF CHEMISTRY

www.rsc.org/catalysis

Catalysis Science & Technology

ARTICLE

Role of Lattice Oxygen on CO Oxidation Over $Ce^{18}O_2$-Based Catalyst Revealed Under Operando Conditions.

Received 00th January 20xx,
Accepted 00th January 20xx

DOI: 10.1039/x0xx00000x

www.rsc.org/

Bartosz Penkala [a b], Daniel Aubert[b], Helena Kaper[b], Caroline Tardivat[b], Kazimierz Conder[c] and Werner Paulus[a].

Ceria-based materials are today the most prominently used catalyst supports for CO oxidation and NO_x reduction in three way catalytic converters (TWC) worldwide. Acting as oxygen buffer compounds, the underlying reaction mechanism and especially the distinct role of surface and lattice oxygen for catalytic reactions, is still under debate. This is partially related to the complexity of the real CeO_2 surface, containing important amounts of water and carbonates. Combining TG-MS, Raman spectroscopic experiments and Isotope Labeling Pulse Temperature Programed Oxidation Reaction (ILPOR), coupled with mass spectrometric analysis on ^{18}O doped ceria, we explored here the oxygen uptake/release behavior under operando conditions, together with the catalytic activity related either to surface and/or lattice oxygen mobility and exchange. Specific changes in the lattice dynamics induced by $^{18/16}O$ isotope exchange were analyzed by Raman spectroscopy, allowing studying selectively the temperature dependent onset of lattice oxygen mobility and isotope exchange behavior. For Pt-supported nano-ceria we evidenced high catalytic performances for CO oxidation, activated slightly above ambient conditions without significant lattice oxygen participation. The distinct role of surface and lattice oxygen in the catalytic reaction of ceria catalysts is discussed as a function of temperature, grain size, Gd-doping and Pt impregnation.

INTRODUCTION

Due to their importance for many technological applications, e.g. TWC in automotive engines,[1-5] photocatalysis,[6-8] solid oxide fuel cells (SOFC),[9-11] oxygen permeation membranes,[12, 13] sensors[14, 15] and biomedical application,[16, 17] ceria-based oxides belong to the most investigated materials. General performances can be tuned and controlled by cation doping, as well as a given microstructure and morphology. Basically ceria adopts the cubic Fluorite-type structure, with cations occupying f.c.c. positions and anions on all tetrahedral lattice sites.[18] The phase diagram of $CeO_{2-\delta}$ is, however, much more complex, revealing a number of phases with oxygen defects under reducing condition.[18-26] Several oxygen deficient $CeO_{2-\delta}$ phases forming complex superstructures in the range of $0 < \delta < 0.5$ have been evidenced by single crystal neutron diffraction.[27] Furthermore, ceria can be synthetized in various morphologies, like nanowires,[28-30] nanotubes,[31-33] 3DOM structure[34] etc., each of them related to specific properties in different fields of application.[35] Its surface catalytic and oxygen buffer properties, oxygen storage capacity (OSC) and oxygen bulk mobility are strongly depending on a dopant specific defect structure of CeO_2, which varies as a function of temperature, oxygen partial pressure,[36-38] electric field,[39] surface stress and quantity of dopants.[40]

A detailed understanding concerning the underlying reaction mechanism of oxygen uptake and release, coupled to its catalytic activity and respective interplay of associated gas-solid redox equilibra is still lacking. In this context we intend to investigate the catalytic activity of ceria and ceria based compounds, with one of the most extensively studied reaction in the field of heterogeneous catalysis, i.e. the oxidation of CO to CO_2.[41, 42] Depending on the oxygen species involved in the catalytic reaction, CO oxidation has been described by the Eley-Rideal,[43] Langmuir-Hinshelwood[44] and Mars-van Krevelen[45] mechanism. It is widely suggested that CO is combining with lattice oxygen on ceria through Mars-van Krevelen Mechanism.[46] Bera[47] and Priolkar[48] proposed that interaction of ceria with Pd and Pt can lead to the dual site mechanism of CO oxidation, the best described by Langmuir-Hinshelwood mechanism.[49]

Our specific interest here is to study the CO oxidation mechanism on highly active nano-Ceria and Ceria based compounds with a special focus on the role of surface and lattice oxygen and related oxygen mobility during the catalytic reaction under dynamically modulated redox equilibra, using a panoply of ^{18}O isotope labeling techniques. We investigated in parallel, complementary temperature dependent oxygen

[a] University of Montpellier, Institut Charles Gerhardt, UMR 5253, C2M, 5 Place Eugene Bataillon, F-34095, Montpellier, France Address here.
[b] Ceramic Synthesis and Functionalization Laboratory, Saint-Gobain CREE, 550 av. Alphonse Jauffret, F-84306, Cavaillon, France
[c] Laboratory for Developments and Methods, PSI, CH-5232 Villigen, Switzerland
† Supplementary Information (ESI) available: [XRD results; Raman Spectra as a function of laser power; ex-situ Raman Spectra; Classical Catalytic Oxidation of CO; RT Raman Spectra]. See DOI: 10.1039/x0xx00000x

mobility by ^{18}O isotope labeling techniques, like thermogravimetric studies coupled with mass spectrometry (TG-MS). These results are then compared to temperature-controlled Isotope LAbeling Raman Spectroscopy (ILARS), allowing accessing specific information for lattice oxygen only. The 18O lattice oxygen participation to the catalytic reaction was determined by Isotope Labeling Pulse Temperature Programed Oxidation Reaction (ILPOR) of CO, giving access to oxygen release and uptake kinetics under dynamic and alternating redox conditions. The latter techniques are reported here for the first time.

EXPERIMENTAL

Fluorite-type nano powders of composition CeO_2 and $Ce_{0.8}Gd_{0.2}O_{1.9}$ were prepared by soft chemistry method. Stoichiometric amounts of $Ce(NO_3)_3*6H_20$ (Sigma Aldrich >99,9%) and $Gd(NO_3)_3*6H_20$ (Sigma Aldrich >99,9%) were dissolved in isopropanol and stirred during 3 hours. This solution was dried at 100°C during 96 h. Resulting powders were calcined with a heating ramp of 1.7K/min to 500°C or 800°C (holding time of 5 h). Temperature variation of the final calcination allowed to control the particle size, i.e. 9 nm CeO_2 (NCEO), 9 nm $Ce_{0.8}Gd_{0.2}O_{1.9}$ (NCGO), were calcined at 500°C and 81 nm CeO_2 (BCEO) and 61 nm $Ce_{0.8}Gd_{0.2}O_{1.9}$ (BCGO) were calcined at 800°C. Impregantion of ceria with Pt was prepared by dissolving stoichiometric amount of $Pt(NO_3)_2$ in ethanol and added dropwise to nano ceria powder, followed by drying at 100°C and calcination at 500°C during 15h and 2h respectively, under air.

Isotope $^{16}O/^{18}O$ exchange was performed for the nano-sized ceria by placing 400 mg of the sample in the quartz reactor under 1 bar atmosphere of $^{18}O_2$ at 400°C. The $^{18}O_2$ gas volume was three times renewed leading to the enrichment in ^{18}O of about 65 %. The exchange reaction was identical for the bulk samples, except the temperature was raised to 500°C.

X-ray Diffraction (XRD) analysis was performed for all oxides using a PANanalytical Empyrean system with PIXcel^{3D} detector operating in Bragg-Brentano Geometry (Θ/2Θ) and $CuK_{\alpha1,2}$ (45kV and 40 mA) radiation. **Fig. S1** resumes all diffractograms for compounds used here, together with their lattice parameters.

TG-MS measurements were carried out on a NETSCH thermobalance Jupiter STA 449C, equipped with a PFEIFFER VACUUM ThermoStar mass spectrometer (MS) using heating rate 5K/min under 20%O_2 in He atmosphere.

Raman Spectra were taken by Raman microscope LabRam ARAMIS IR2 with 1800-line mm^{-1} diffraction grating and a charge coupled device camera cooled by a thermoelectric Peltier device (CCD) detector using a D473 - 473 nm and HeNe - 633 nm diode-pump solid state laser and D1 filter (10% power). Samples were placed on a platinum support in the Linkam TS1500 heating stage under the objective (X50) of the microscope. The temperature was measured by a thermocouple at the bottom of the oven. Raman spectra were taken every 100°C, in the temperature range between RT and 650°C. We checked for a possible influence of the laser power on the thermal stability of the measured samples, showing no laser induced damages or local overheating effect, see **Fig. S2**. Moreover ^{18}O NCGO enriched samples, which were preheated ex-situ to 250°C, indicated by Raman spectroscopy at ambient truly temperature induce isotopic oxygen exchange, excluding possible laser overheating, see **Fig. S3**.

In order to determine possible correlations between oxygen mobility and catalytic activity during the CO oxidation test reaction, ILPOR was carried out in an Automated Catalyst Characterization System (Autochem II 2920) coupled with quadruple mass spectrometer (QMS) (Thermostar TM GSD 301T Pfeiffer Vacuum). 100 mg of an ^{18}O enriched sample was loaded in a U-shape micro reactor system and stabilized at 40°C under $^{16}O_2$ (16 cm^3/min) atmosphere, approximately during 1 hour. Once stabilized, the reactor temperature was raised to 500°C with a ramp of 2K/min. The carrier gas used was 1%$C^{16}O$/He (16 cm^3/min, 10 000ppm) to which pulses of $^{16}O_2$ with a volume of 0.5785 cm^3 were injected by the loop valve every 60 s with an injection time of 0.2 µs (corresponding to 50 000 ppm O_2 on average). The evolution of different oxygen isotopes containing species (m/e = 16 for $^{16}O^-$, m/e =17 for $^{16}OH^-$, m/e = 18 for $^{18}O^-/H_2{}^{16}O$, m/e = 19 for $^{18}OH^-$, m/e = 20 for $H_2{}^{18}O$, m/e = 28 for $C^{16}O$, m/e = 30 for $C^{18}O$, m/e = 32 for $^{16}O_2$, m/e = 34 for $^{16}O^{18}O$, m/e = 36 for $^{18}O_2$, m/e = 44 for $C^{16}O^{16}O$, m/e = 46 for $C^{16}O^{18}O$, m/e = 48 for $C^{18}O^{18}O$) were monitored by the QMS during the temperature programed oxidation of CO. Pt-impreganted CeO_2 was H_2 activated at 300°C during 2h followed by cooling down under He atmosphere prior to the ILPOR measurement.

RESULTS

Regarding ceria as an oxygen buffer compound, it is obvious that the oxygen release and uptake performance together with bulk oxygen mobility, affects catalytic activation processes. The question, which type of oxygen species are involved in the catalytic reaction, is still controversially discussed, as it remains a challenge to distinguish between the implication of surface and/or bulk oxygen.

In order to access surface and bulk oxygen participation for the catalytic reaction we combined three complementary characterization techniques, namely TG-MS, Raman spectroscopy and a pulsed catalytic reaction. The latter was carried out under *operando* conditions during the $C^{16}O$ oxidation on ^{18}O-enriched ceria. To access the influence of Gd-doping, grain size and Pt-impregnation, we used pure NCEO, BCEO, NCGO and BCGO as well as 9 nm grain size CeO_2 impregnated by 2.5% in weight of Pt.

The catalytic results on non-stoichiometric ceria will be compared to the catalytic activities of $CaFeO_{2.5}$ with Brownmillerite type structure, which we found has equal catalytic potential for CO oxidation at very moderate temperatures, see **Fig. S4**.[50] In contrast to ceria, $CaFeO_{2.5}$ is a stoichiometric line phase, allowing differentiating in a complementary way between lattice and surface oxygen participation, as further outlined below.

Since TG-MS gives solely an integral weight change of the sample, it is impossible to discriminate between different oxygen species released from the surface or bulk. Using Raman spectroscopy, changes in the lattice dynamics related to the replacement of ^{18}O by ^{16}O during heating under $^{16}O_2$-atmosphere provide selective lattice oxygen information. To better access CO oxidation performance during ILPOR, we supplied molecular oxygen by a pulsed injection instead of a continuous flow, allowing to better differentiating dynamic exchanges with the bulk and surface interface. As the partial pressures of CO and O_2 are periodically altered, the system is exposed to reducing or oxidizing atmosphere. Thus, a pulsed oxygen injection allows not only to monitor, as outlined in more detail below, a rapid oxygen release/uptake behavior, but to decisively discriminate contributions related to true bulk oxygen diffusion.

TG-MS

TG-MS analysis of $Ce^{18}O_2$ and $Ce_{0.8}Gd_{0.2}{}^{18}O_{1.9}$ samples with varying crystalline size are shown in **Fig. 1**. The first significant weight loss of 1.5% for both NCEO and NCGO is observed between 25 and 200°C while for BCEO and BCGO a weight loss of only 0.5% is observed in the same temperature interval. Mass spectrometry data support the assignment of this mass decrease to the loss of weakly adsorbed water. Unfortunately, the mass of H_2O and $^{18}O^-$ are identical, however, in the case of $^{18}O^-$ one would expect to observe a simultaneous formation of $^{18/16}O_2$ molecules, which reasonably rules out this option. The second major weight loss of about 1.5% is observed between 400 and 600°C, corresponding to the quantitative exchange of ^{18}O from the lattice with $^{16}O_2$ from atmosphere, forming $^{18/16}O_2$ and $^{18}O_2$ species. While for 100% ^{18}O enrichment a weight loss of 2.3% is expected, the enrichment achieved here yields 65%. The same weight loss corresponding to ^{18}O is accompanied by an MS signal corresponding to m/e = 18, which is attributed to monoatomic $^{18}O^-$ ions. This signal is less significant for NCEO and NCGO, while it becomes more important with increasing grain size. This might be related to a more facile recombination to molecular oxygen in case of higher surface area.

While for NCEO and NCGO samples the temperature of quantitative oxygen isotopomers exchange takes place at 400°C, a shift towards 500°C is observed in case of BCEO and BCGO. This tendency, i.e. the variation of the onset behavior even when using isotopes, and especially for the nano-sized catalysts. We want to underline that an important catalytic activity is found already in the temperature region below 400°C, i.e. before oxygen isotope exchange sets in, together with the presence of a pronounced surface coverage with water, as further outlined below.

Raman

In order to analyze selectively the exchange behavior of lattice oxygen as a function of temperature, we studied the changes of lattice dynamics for the oxygen related F_{2g} Raman mode, related to the mass difference of $^{18}O/^{16}O$ isotopes, **Fig. S5**.

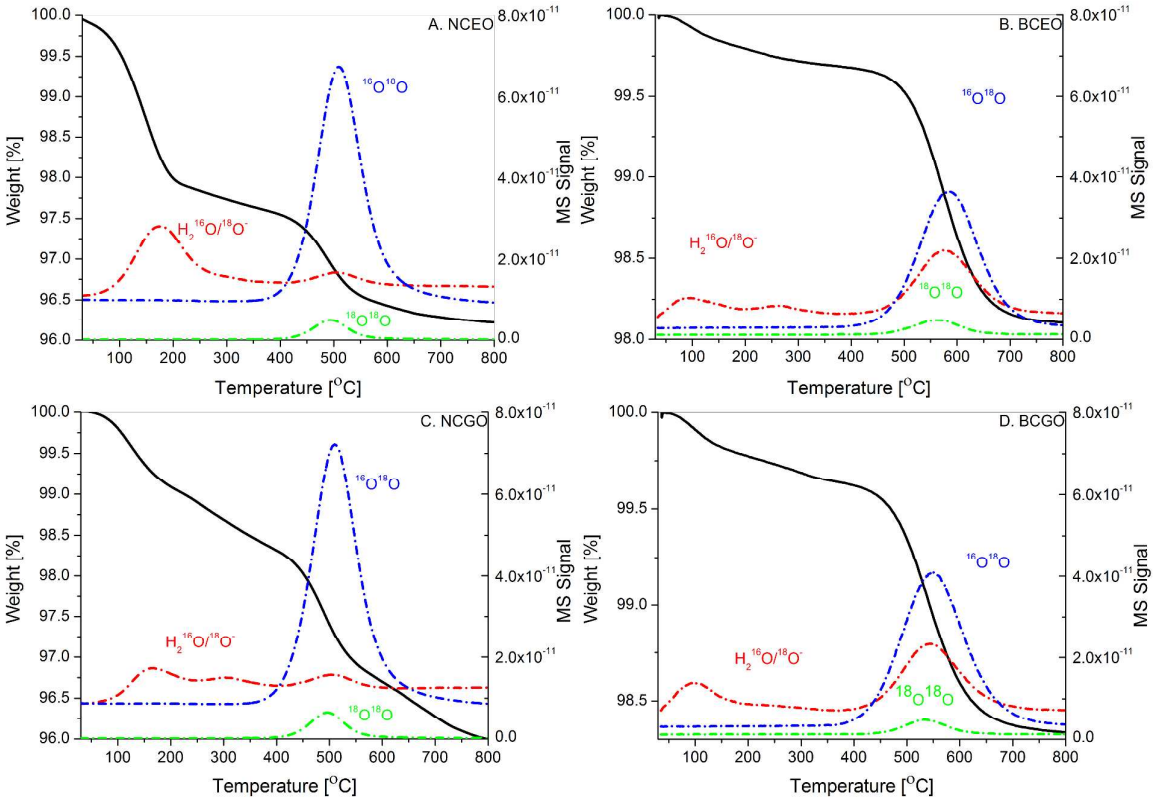

Figure 1 Thermogravimetric-mass spectroscopic study of: A. NCE^{18}O 9 nm; B. BCE^{18}O 81nm; C. NCG^{18}O 9 nm; D. BCG^{18}O 61 nm, using a heating rate of 5K /min in 20%$^{16}O_2$/He gas atmosphere. A mass change of 2.3% would be expected in case of a 100% ^{18}O enriched sample. As becomes evident from the MS signal, all mass

losses below 400°C belong to the desorption of loosely bound water, while a quantitative oxygen isotope exchange requires at least temperatures of 400°C or above. The amount of water content is significantly higher in case of NCE^{18}O and NCG^{18}O compared to the respective bulk samples.

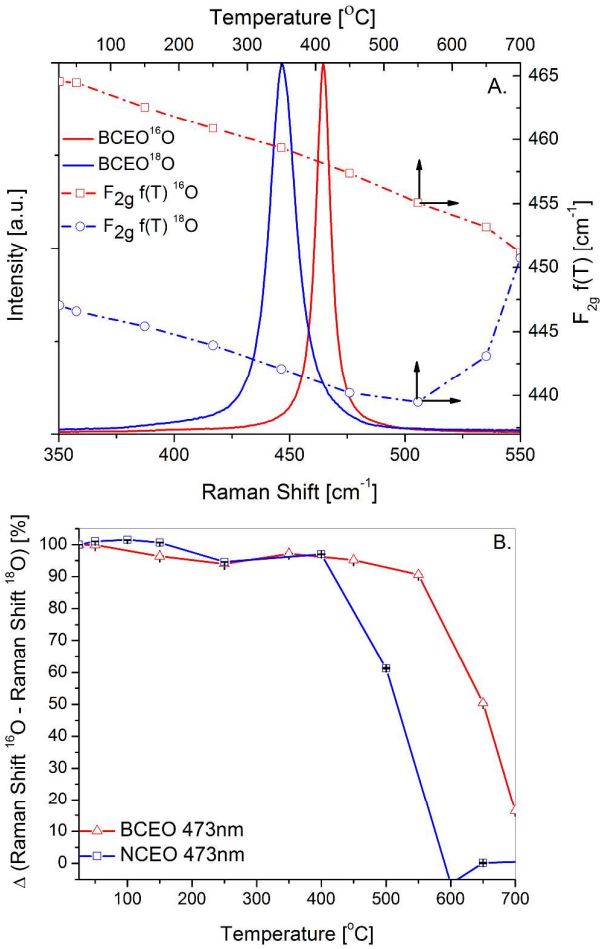

Figure 2 A. F_{2g} Raman mode position for $Ce^{16}O_2$ with 81 nm (red solid line) and $Ce^{18}O_2$ with 81 nm (blue solid line) obtained at ambient temperature with an incident wavelength of λ = 473 nm. The dashed-dotted lines in the respective colors show the T-dependent shift of the F_{2g} Raman modes obtained in air as a function of temperature, while their differences Δ = $\nu(^{16}O)$ - $\nu(^{18}O)$ are shown in Fig. 2B as a function of temperature for CeO_2 with 81 nm (red line) and nano-CeO_2 with 9 nm grain size (blue line). This method, which is sensitive to lattice oxygen only, yields onset temperatures for $^{18}O/^{16}O$ exchange of 550°C for BCEO, while it decreases to 400°C for NCEO.

Analyzing the change in the Raman frequency shift of the CeO_8 breathing mode, assigned as the F_{2g} mode around 446 cm^{-1}, during heating up ^{18}O-enriched ceria in a $^{16}O_2$ atmosphere, will thus allow concluding on the $^{18}O/^{16}O$ ratio and respective exchange behavior.

In **Fig. 2A**, the F_{2g} peak positions of ^{16}O- and ^{18}O-enriched 81 nm sized CeO_2, indicate a difference of 17cm^{-1} at ambient temperature. The change in the peak position as a function of temperature is overlaid in the same figure for samples containing ^{18}O and ^{16}O isotopes. Both F_{2g} frequencies change continuously with a constant gap up to 550°C while above this temperature, the F_{2g} Raman mode of the ^{18}O enriched BCEO sample shows a significant deviation towards higher frequencies, finally approaching the signal measured for the pure ^{16}O sample.

The difference of both signals is a direct quantitative measure for the $^{18}O/^{16}O$ isotope exchange ratio, which is used in **Fig. 2B** to indicate the $^{18}O/^{16}O$ exchange rate taking the difference of both signals. Using Δ = $\nu(^{16}O)$ - $\nu(^{18}O)$ at room temperature as the starting point and set to 100%, Δ stays invariant within 5% up to 400°C for both compounds NCEO and BCEO, indicating that no lattice oxygen isotope exchange takes place within this temperature range. Since the slope of the Raman frequency for both, ^{16}O and ^{18}O containing isotopes is identical with temperature, the difference (Δ) of the vibrational energies between both isotopomeric samples at a given temperature reflects only changes of the vibrational energy related to isotopic exchange. Systematic errors originating e.g. from temperature-induced volume expansion and anharmonicity effects are thus minimized.[52, 53] Following the variations of Δ with temperature, we observe a steep change above 400°C for NCEO, while for BCEO, Δ starts to vary around 550°C. Both values are in agreement with TG-MS measurements discussed above, confirming the temperatures obtained for oxygen isotope exchange reactions and the ability of this method to selectively monitor lattice oxygen exchange behavior.

Catalysis

In general CO-oxidation is studied employing a constant gas flow of CO/O_2 gas and analyzing the reaction products by mass spectrometry (MS), gas chromatography, or similar. Here, we want to specifically address the participation of surface and/or bulk lattice oxygen to the reaction by ILPOR. This method uses ^{16}O-pulses added to a constant C^{16}O flow as a function of temperature over ^{18}O-enriched ceria. This set-up allows following in real time the catalytic activity under a periodically swinging redox potential over ^{18}O-enriched ceria, and which consequently provides via the related oxygen exchange, uptake and release kinetics, valuable information on the underlying reaction mechanism. Following the overall gas concentrations outlined above (see experimental section), the total molar oxygen quantity is on an overall scale about five times higher compared to CO. The catalytic oxidation of CO to CO_2 can occur via two distinct reaction mechanisms.

The first one is the direct oxidation of CO using lattice oxygen, leaving behind oxygen-deficient $CeO_{2-\delta}$, which can be re-oxidized by O_2-uptake from the air. The second one is the reaction of CO with the injected O_2 from the gas atmosphere on the ceria surface. Since both reactions are supposed to proceed at the surface of the catalyst, it is *a priori* difficult or almost impossible, to unambiguously specify the origin of the involved oxygen atoms and hence to conclude on the reaction mechanism. Additional complexity arises from the fact that ceria becomes non-stoichiometric at already moderate temperatures, and thus able to undergo $^{18}O/^{16}O$ oxygen isotope exchange reactions as outlined above. Since both reactions are partially overlaid, it is in principle difficult to access towards a quantitative understanding of the reaction mechanism and involved oxygen atoms. We aimed to

overcome these difficulties, accessing the participation of lattice or surface-bound gas phase oxygen to the catalytic reaction, via a periodic modulation of an applied redox potential between CO and O_2 on the catalyst and to focus on dynamically analyzing related reaction products and, to a certain extend, associated kinetics. The studied system is thus quite complex, as together with a continuously increasing temperature, we add a periodically oscillating redox potential via variations of the CO/O_2 atmosphere. However, this set-up will allow at least on a qualitative level, to follow up oxygen uptake/release behavior and to access in parallel the impact of lattice oxygen on the catalytic reaction.

The employed pulsed structure for the $^{16}O_2$-injection is balanced here in a way that the resulting modulation of the oxygen partial pressure and related oxygen exchange kinetics with/at the catalyst, allows to dynamically discriminate between the implication of bulk and surface oxygen through the formation of $C^{16}O^{18}O$ and, to a minor extent, $C^{18}O^{18}O$, **Fig. 3**. We first report the results of $CaFeO_{2.5}$ with Brownmillerite structure, which may serve as a reference, related to the fact that it presents a stoichiometric line phase under the employed reaction conditions.

Temperature-dependent activation of $^{18}O/^{16}O$ oxygen isotope exchange for $CaFe^{18}O_{2.5}$, performed as a solid-gas exchange reaction in $^{16}O_2$ atmosphere, has been shown to strongly depend on the grain size, as outlined above.[51] Employing 40 nm size $CaFeO_{2.5}$, we observed during ILPOR the formation of 3 different CO_2 isotopomers namely $C^{16}O^{16}O$, $C^{16}O^{18}O$ and $C^{18}O^{18}O$ above 250°C. The oxidation to CO_2 is accompanied by a corresponding reduction of the $^{16}O_2$ signal, indicating that the oxygen from the gas atmosphere is used for the CO_2 production, see **Fig. 4**.

Formation of $C^{16}O^{18}O$ in parallel to pure $C^{16}O^{16}O$ is related to the fact that oxygen starts to get mobile in $CaFeO_{2.5}$ at these temperatures, creating to a certain extend an oxygen isotope exchange system, where oxygen is almost freely diffusing inside the Brownmillerite matrix. We note that the MS signal of all CO_2 species is exactly modulated with the pulsed MS signal of $^{16}O_2$, confirming dynamically the direct involvement of the provided oxygen gas in the reaction chamber for the CO oxidation.

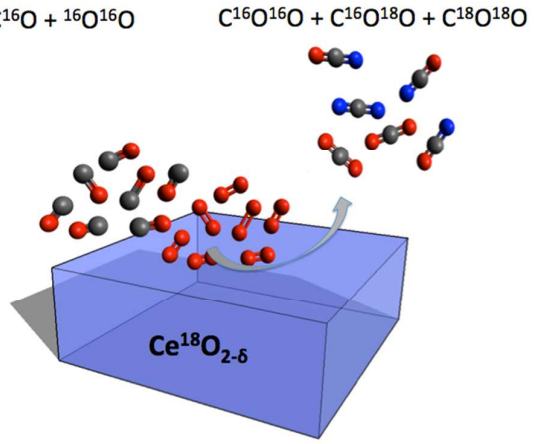

Figure 3 Schematic view of the $C^{16}O$ oxidation at the $Ce^{18}O_2$ interface, carried out using a $^{16}O_2$ oxygen pulse on top of a continuous 1%$C^{16}O$/He gas flow. The 3 different CO_2 isotopomers formed, namely, $C^{16}O^{16}O$ and $C^{16}O^{18}O$, $C^{18}O^{18}O$ are analyzed by time-resolved mass spectrometry with respect to the underlying $^{16}O_2$ pulse structure (cf. text).

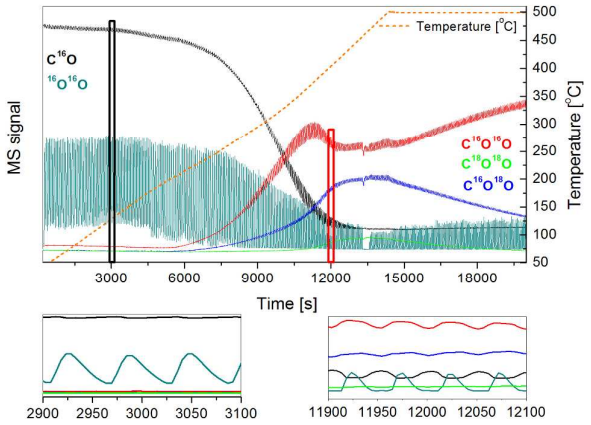

Figure 4 ILPOR plot obtained for nano-$CaFeO_{2.5}$. While heating the temperature of the reactor vessel by 2K/min, $^{16}O_2$ pulses were injected periodically to a constant carrier gas of 1%CO/He, causing symmetrical oscillating $^{16}O_2$ MS signals (green line). The relatively small oscillations of the $C^{16}O$ signal (as well as CO_2 signals) are related to local fluctuation of its partial pressure caused by the $^{16}O_2$ pulses. In parallel the three possible MS signals for $C^{16}O^{16}O$, $C^{16}O^{18}O$ and $C^{18}O^{18}O$ (light green, blue and red curves) are monitored together with the $C^{16}O$ signal (black curve), as a function of the reaction time and –temperature. The zoomed sections at the bottom allow following the pulsed structure of all signals and respective relative quantities. From the coherence of the $^{16}O_2$ and all CO_2 signals we can conclude on a direct $^{16}O_2$ turnover during the catalytic reaction.

Reaching the maximum reaction temperature at 500°C (eq. 14000 s), which is then kept constant, as further increase would modify the $CaFeO_{2.5}$ microstructure and thus the grain size, we observe a continuous decrease of the $C^{16}O^{18}O$ signal, while the $C^{16}O^{16}O$ signal accordingly increases. This is a consequence of a progressive ^{18}O concentration reduction in the lattice with reaction time.

Coming to the catalytic activity of ceria, the situation becomes more complex. This is related to the fact that ceria can act as an oxygen buffer and thus becomes non-stoichiometric with temperature and especially under reducing reaction conditions, while its catalytic surface activity depends on the availability of active centers, i.e. oxygen vacancies, as discussed elsewhere.[54] Looking at the CO_2-MS signals for NCEO (see **Fig. 5A**), CO conversion sets in above 250°C with the overall CO_2 signal intensity continuously increasing with temperature. At about 300°C the CO_2 signal starts to oscillate around its equilibrium value, at a CO concentration corresponding to almost half of its initial value. On an overall scale the concentration of $C^{16}O^{18}O$ goes through a maximum around 400°C, while it further decreases with temperature. This confirms as already discussed above for the TG studies, that oxygen isotope exchange is fully activated at 400°C and enables all lattice ^{18}O to participate to the catalytic reaction. The $C^{16}O^{16}O$ signal increases accordingly with the decrease of the $C^{16}O^{18}O$ signal. Inspecting in more detail the $C^{16}O^{16}O$ and $C^{16}O^{18}O$ oscillations in the region between 12160 and 12260 sec, we can state that both follow the same oscillation characteristics, which are, however, not as regular as observed for $CaFeO_{2.5}$ discussed above. Each steep increase of the CO_2 signal is followed by a longer smooth decrease as given in the magnified part in **Fig. 6**. What is even more intriguing is the

fact that the steep increase of the CO_2 signal is, independent of the $C^{16}O^{18}O$ isotope composition, starting, before the O_2-pulse initiates.

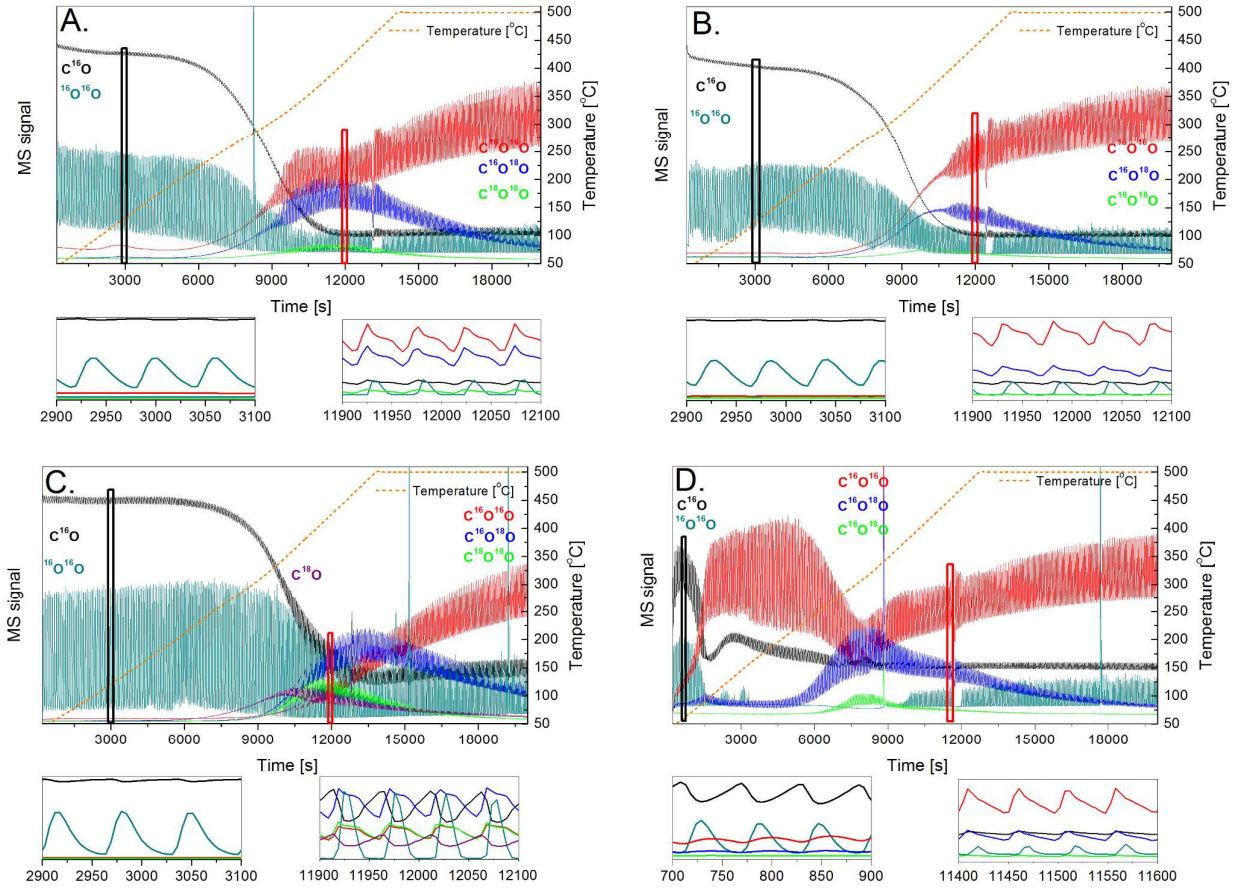

Figure 5 ILPOR plots for: NCE^{18}O (A), NCG^{18}O (B), BCG^{18}O (C) and 2.5% wt. Pt-impregnated NCE^{18}O (D). For all experiments a heating rate of 2K/min was used. The $^{16}O_2$ oscillations at the beginning of the reaction reflect the $^{16}O_2$ pulses added to the 1%$C^{16}O$/He carrier gas. The CO_2 oscillations setting in for NCE^{18}O at 300°C and for NCG^{18}O around 375°C are related to the formation of non-stoichiometric $CeO_{2-\delta}$ or $Ce_{0.8}Gd_{0.2}O_{2-\delta}$ and associated oxygen uptake and release behavior. From the time resolved O_2 pulse structure, the steep increase of the CO_2 signals is observed for both compounds to set in already before the oxygen pulse arrives at the sample (see also the magnified part in Fig 6), indicating lattice oxygen as source for the catalytic reaction, while creating non-stoichiometric ceria. The subsequent smooth decrease corresponds to a superposition of oxygen uptake with the catalytic reaction, which is ongoing in parallel. The $C^{18}O^{16}O$ formation without oscillations in (A) and (B) indicates direct oxygen turnover strongly involving near surface oxygen, which amounts for nano-sized ceria to 30% of the total oxygen. We note for BCGO the absence of a catalytic activity without CO_2 oscillations as indicated in (C). In (D) a strong catalytic activity becomes evident for 2.5% wt. Pt-impregnated NCEO by strong CO_2 oscillations starting just above ambient, consuming directly almost all supplied $^{16}O_2$. The oscillations are here consequently not related to a "breathing-behavior" as found for NCEO, but directly following the $^{16}O_2$ supply.

It is thus evident, that the oxygen for the CO oxidation is, at this moment, not originating from the gas in the reaction vessel, but from the lattice of ceria itself. We may thus conclude that the oxidation mechanism involves lattice oxygen atoms from ceria, thus creating oxygen vacancies and yielding non-stoichiometric $CeO_{2-\delta}$. Once the maximum of the CO_2 peak is achieved, it decreases smoothly in intensity, which we interpret to be related to a competitive interplay of the ongoing catalytic reaction of CO, while at the same time, oxygen provided by the O_2-pulse, also directly serves for the re-oxidation of ceria. For clarity we added in **Fig. 6** the oxygen pulse time structure as observed at the beginning of the experiment (time scale between 3160 and 3260 sec, marked by dashed-dotted line), where no catalytic activity is observed. The full width of the initial pulse reduces significantly at higher temperatures due to oxygen consumption related to the formation of CO_2. For $CaFeO_{2.5}$, the oscillations were found on a considerably lower scale. The strong oscillations observed for CeO_2 can thus be interpreted to be at least partially related to the non-stoichiometry of ceria and the amplitudes then reflect the "breathing-behavior" of ceria. The region below 300°C, where catalytic activity is observed, but without significant oscillations of CO_2, must be interpreted to essentially rely on a high surface catalytic activity, directly involving the oxygen from the O-pulse for CO oxidation. Also for this temperature range we observe the formation of a $C^{16}O^{18}O$ signal, equally proving a direct implication of the lattice oxygen. It remains questionable, to which extend this is related to partial oxygen mobility of the near surface region and thus allowing a limited $^{18}O/^{16}O$ exchange reaction, or induced by the strong and oscillating redox potential of the CO/O_2 pulse structure. While the catalytic behavior of Gd-doped ceria is similar to pure ceria, the temperature for oscillations to set in is shifted to 375°C, which is significantly higher compared to NCEO, **Fig. 5B**. We note, however, that the appearance of oscillations seems to be much better defined than for undoped ceria. Below

375°C, we conclude from the low/absent oscillation amplitudes, together with a high CO conversion rate, on a high

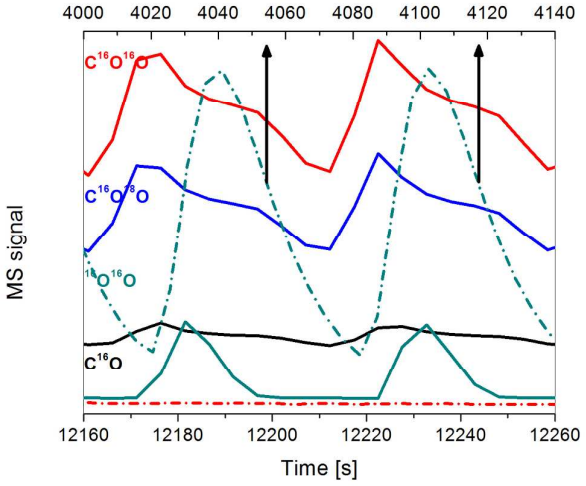

Figure 6 Pulse-depended conversion of CO to CO_2 for NCE^{18}O (solid red, blue and green lines) with pulses obtained at a time scale between 12160 and 12260s, i.e. with catalytic activity, and for $^{16}O_2$ pulses by a dashed-dotted green line corresponding to part of the reaction without catalytic activity (4000-4160 s), while the dashed-dotted red line corresponds to the CO_2 signal in the same region. The figure is a magnified part of Fig. 5A.

surface catalytic activity also including high dynamic lattice ^{18}O exchange capacity, as already discussed for the pure CeO_2 sample.[55] This behavior is somehow expected, as Gd-doped ceria intrinsically contains a higher concentration of oxygen defects compared to CeO_2, which act as active catalytic centers. It is astonishing to note that the $C^{16}O^{18}O$ signal follows the $C^{16}O^{16}O$ signal, even in the region with low oscillations, where high CO conversion is observed, at which the $C^{16}O^{18}O$ signal reaches already its maximum. It becomes thus clear that an important amount of the lattice ^{18}O is participating to the CO oxidation. It is worth to note that the use of 9 nm grain size CGO implies an important quantity of near surface ^{18}O atoms available for the reaction. Assuming that the ^{18}O lattice oxygen participation for the formation of $C^{16}O^{18}O$ is induced by the modulated redox potential, i.e. the pulsed CO/O_2 structure, the supposed volume for ^{18}O-transfer, taking into account a thickness of 2 unit cells starting from the surface of a 9 nm grain, amounts to around 30% with respect the to total sample volume. This implies an important amount of the lattice oxygen is readily available for exchange in the presence of CO at 250°C, without the necessity for ceria to become non-stoichiometric. This is a significant difference to the $^{18}O/^{16}O$ isotope exchange behaviour, without the presence of strongly reducing agents.

Verifying the importance of the grain size for a possible $^{18}O/^{16}O$ exchange of the surface and subsurface region should consequently become accessible through analyzing the catalytic activity of CGO with a larger grain size. This allows not only concluding on possible changes for the kinetics of the dynamic oxygen exchange capacity (OEC), but equally on the oscillation behavior related to the competitive interplay of the different redox reactions involved. Besides the CO oxidation to CO_2, this also concerns the re-oxidation of possible oxygen vacancies in ceria, in addition to defects related to Gd-doping.

From the catalytic activity of BCGO, as illustrated in **Fig. 5C**, we first note the absence of a region with low CO_2 oscillations. As a consequence we conclude on a strongly reduced catalytic activity for the CO oxidation, when compared to NCGO. On the other hand, a relevant oscillation free signal for $C^{18}O$ comes up already before the CO_2 conversion sets in. The onset of CO oxidation goes directly along with the onset of $C^{16}O^{18}O$ oscillations, indicating that lattice oxygen is strongly involved in the oxidation reaction, creating oxygen defects in BCGO. This is also supported by the modulation of the CO_2 signal, similar to what was observed for pure CeO_2. A limitation in the dynamic OEC becomes visible through a steep increase of the CO_2 signal, which herein relaxes much more smoothly to its starting value as clearly indicated in the intersection of **Fig. 5C**. The different CO_2 oscillation behavior comparing 9 nm NCGO and 61 nm BCGO are thus related to a drastic change in the dynamic exchange capacity, which is then governing the kinetics of the two main reaction equilibrium involved, i.e. the CO oxidation on one hand and the re-oxidation of CGO on the other hand. The reduced ^{18}O dynamic exchange behavior for 61 nm BCGO is also expressed by the $C^{16}O^{18}O$ signal reaching a maximum at 450°C, while 350°C are observed for the 9 nm NCGO. The same conclusion can be obtained following the CO conversion setting in at 320°C and 220°C for the 61 nm and 9 nm samples respectively, reaching completeness at 500°C and 400°C.

While all catalytic reactions so far were investigated without using noble metals, we consider now Pt-impregnated nano-sized ceria, in order to study its catalytic influence and especially concerning the participation of lattice oxygen to the catalytic reaction. As indicated in **Fig. 5D**, a complete different scenario for the catalytic activity is observed for a 2.5%wt. Pt impregnated nano-ceria with 9 nm grain size, and 1 nm sized Pt. High catalytic activity, already starting below 50°C, is indicated by the rapidly decreasing CO signal. Above 100°C, CO_2 oscillations are strongly increasing in the absence of a $C^{16}O^{18}O$ signal, proving that all provided oxygen gas in the reaction vessel is directly used for the CO conversion, supporting the Langmuir-Hinshelwood mechanism. The CO_2 oscillations are here not a result of ceria non-stoichiometry and associated "breathing-behaviour", but a consequence of a complete O_2 turnover, the variations in the CO_2 signal are thus directly monitoring the O_2-availability. Almost no ^{18}O lattice oxygen participation is observed below 250°C, except for a very small hump in the $C^{16}O^{18}O$ signal, which comes along with the inset of increased $C^{16}O^{16}O$ oscillations at around 100°C. We can see that this contribution is not observed for any of the pure ceria supports. This minor contribution might be attributed to the formation of highly active $^{18}O/Pt_8/Ce_{40}{}^{18}O_{79}$ species as described in[56], following reverse oxygen spillover from ceria onto the platinum species, and subsequent reaction with CO, forming $C^{16}O^{18}O$ species at low temperatures. In any case we observe a direct correlation of the CO_2 pulses with the O_2 modulation, which indicates a one-step Langmuir-Hinshelwood type oxidation mechanism. It remains so far

unclear whether the oxygen originates from oxygen provided by $^{18}O/Pt/Ce^{18}O_{2-\delta}$-type species or if locally active Pt-^{18}O-Ce bonds serve as active catalyst centres. In both cases, the minimum in the $C^{16}O$ signal around 100°C can be explained by the consumption of ^{18}O derived from highly active species, going along with the appearance of the $C^{16}O^{18}O$ signal.

The fact that seemingly no lattice oxygen participates to the catalytic reaction is in contradiction to what is reported elsewhere, as it implies that the kinetics of CO oxidation over Pt/CeO_2 depends on the partial pressure of O_2, while it has been found to be independent of the oxygen partial pressure[57], at least for low $p(O_2)$ values. The ^{18}O exchange reaction for 2.5%wt. Pt impregnated nano-ceria with 9 nm grain size reported here, clearly indicate at least no quantitative ^{18}O exchange from the lattice sets in below 250°C. In this view we might, however, not exclude to consider the small hump observed at around 100°C, to correspond to an oxygen exchange of the CeO_2/Pt interface, which can serve as an exchange volume which is not negligible, taking into account the surface area and dispersion. The results obtained here might in this way also be perceived as a participation of lattice oxygen (i.e. Mars van Krevelen type), even if it is clear that only a very narrow surface depth is serving for the oxygen exchange reaction, participating to the catalytic reaction.

Increasing the temperature above 100°C leads to a notable reduction in the CO conversion. At the same time, Pt is supposed to get preferentially covered by CO, thus possibly limiting the catalytic reaction rate.

The catalytic activity above 250°C is then following the same trends as observed for pure ceria when lattice oxygen is fully participating to the reaction.

The increase of the $C^{16}O^{18}O$ and $C^{18}O^{18}O$ signal going in parallel along with a decrease of the $C^{16}O^{16}O$ signal, thus indicates a change of the reaction mechanism from Langmuir-Hinshelwood mechanism to the Mars-van Krevelen mechanism, as indicated by a change in the modulation of the $C^{16}O^{18}O$ signal with respect to the $^{16}O_2$ amplitudes.

CONCLUSIONS

This work aims attaining a better fundamental understanding of the role lattice oxygen has in highly active nano-sized ceria based catalysts. Several isotope-labelling techniques were combined in order to explore the catalytic reaction mechanism and especially on how bulk oxygen mobility, and oxygen release and uptake kinetics contributes to the catalytic oxidation of CO to CO_2.

From TG coupled MS studies we were able to show that ^{18}O lattice oxygen exchanges quantitatively only above 400°C, while below this temperature an important amount of loosely bound water is released. The differentiation between oxygen and water release was possible using ^{18}O labelling. These results are confirmed by Raman spectroscopic studies on $Ce^{18}O_2$, selectively probing lattice oxygen only.

Oxygen uptake and release behaviour during the catalytic oxidation of CO to CO_2 became directly accessible, employing periodically alternating redox conditions, realized via $^{16}O_2$-pulses added onto a continuously flowing $C^{16}O$/He carrier. Time-resolved MS was accordingly used to analyse the reaction products, with reference to the initial $^{16}O_2$ pulse structure, while in parallel all catalytic activity was monitored by MS. This allowed following the exchange behaviour of ^{18}O from $Ce^{18}O_2$ towards catalytically formed $C^{16}O^{18}O$, which permitted concluding on the implication of lattice oxygen for the catalytic reaction, as a function of temperature. In this way we could differentiate surface catalytic activity from a reaction involving the formation of non-stoichiometric ceria clearly evidencing buffer behaviour inducing CO_2 oscillations.

While TG and temperature dependent Raman studies on ^{18}O enriched ceria samples result concordantly in temperatures above 400°C for isotope exchange reactions of ^{18}O lattice oxygen with ^{16}O from the gas atmosphere, we evidenced that a significant amount of ^{18}O isotope exchange is induced by the modulated red/ox potential. This results form the $C^{16}O/^{16}O_2$ pulse structure, involving an oxygen exchange volume, corresponding to a thickness of about 2 unit cells below the surface, which for a 9 nm grain amounts to about 30% of its total oxygen content. In this way we were able to demonstrate for NCGO an amplified dynamic OEC and enhanced surface catalytic activity compared to NCEO, indicated by a shift of CO_2 oscillations to set in at higher temperatures. This proves that even at low temperatures the participation of lattice oxygen, which in fact can be identified as lower surface region oxygen, to the catalytic reaction is important at least for nano-sized ceria.

We could evidence a pure catalytic activity and high oxygen turnover, without significant participation of lattice oxygen for Pt-impregnated nano-CeO_2. This catalytic activity sets in at room temperature up to 220°C, while above this limit an increasing exchange of ^{18}O indicates a progressing contribution of lattice oxygen to participate in the catalytic reaction.

The strength of ILPOR for all these investigations is thus to provide a much deeper insight in the catalytic reaction mechanism, compared to classical light off curves only providing integral information, as a dynamic swinging redox potential allows to differentiate between surface and lattice oxygen implication in the same experiment. In this context the formation of non-stoichiometric ceria and related “breathing-behaviour” becomes easily accessible by ILPOR, which is difficult to quantify by other methods.

Summarizing, this dynamical approach is, although inherently much more complex to interpret, essentially due to the overlay of different redox equilibra, much more appropriate to analyse, to which extent lattice oxygen contributes to the catalytic reaction.

Acknowledgements

We acknowledge the financial support of the ANRT (Association National Recherche Technologie) and Saint-Gobain through a CIFRE fellowship, convention 2012/1017.

References

1 A.Trovarelli, C. Leitenburg, M. Boaro, G. Dolcetti, Catal. Today 1999, **50**, 353-367.
2 S. Bedrane, C. Descorme, D. Duprez, Catal. Today 2002, **75**, 401-405.
3 G. Kim, Ind. Eng. Chem. Prod. Res. Dev. 1982, **21**, 267-274.
4 F. Deganello, A. Martorana, J. Solid State Chem 2002, **163**, 527-533.
5 A. Martorana, G. Deganello, A. Longo, A. Prestianni, L. Liotta, A. Macaluso, G. Pantaleo, A. Balerna, S. Mobilio, J. Solid State Chem 2004, **177**, 1268-1275.
6 J. M. Coronado, A. J. Maira, A. Martinez-Arias, J. C. Conesa, J. Soria, J. Photoch. Photobio. A 2002, **150**, 213-221.
7 N.M. Zholobak, V.K. Ivanov, A.B. Shcherbakov, A.S. Shaporev, O.S. Polezhaeva, A. Ye. Baranchikov, N. Ya. Spivak, Yu. D. Tretyakov, J. Photoch. Photobio. B 2011, **102**, 32-38.
8 Ch. Wang, Y. Ao, P. Wang, J. Hou, J. Qian, J. Hazard. Mater. 2010, **184**, 1-5.
9 A. Tsoga, A. Gupta, A. Naoumidis, P. Nikolopoulos, Acta. Mater. 2000, **48**, 4709-4714.
10 D.L. Maricle, T.E. Swarr, S. Karavolis, Solid State Ionics 1992, **52**, 173-182.
11 A. Atkinson, Solid State Ionics 1997, **95**, 3-4, 249-258.
12 J. Han, Y. Zeng, G. Xomeritakis, Y.S. Lin, Solid State Ionics 1997, **98**, 63-72.
13 H. Takamura, T. Kobayashi, T. Kasahara, A. Kamegawa, M. Okada, J. Alloy Compd. 2006, **408-412**, 1084-1089.
14 P. Jasinski, T.Suzuki, H. U. Anderson, Sensor Actuat. B-Chem. 2003, **95**, 73-77.
15 T. S. Stefanik, H. L. Tuller, J. Eur. Ceram. Soc. 2001, **21**, 1967-1970.
16 K. Byrappa, S. Ohara, T. Adschiri, Adv. Drug Deliver. Rev. 2008, **60**, 299-327.
17 R. Benzaid, J. Chevalier, M. Saadaoui, G. Fantozzi, M. Nawa, L. A. Diaz, R. Torrecillas, Biomaterials 2008, **29**, 3636-3641.
18 R. Martin, J. Chem. Soc. Dalton Trans. 1997, **20**, 3659-3700.
19 S. P. Ray, J. Solid State Chem. 1975, **15**, 333-343.
20 D. J. M. Bevan, J. Kordis, J. Inorg. Nucl. Chem. 1964, **26**, 1509-1523.
21 M. Ricken, J. Nolting, J. Solid State Chem. 1984, **54**, 89-99.
22 S. P. Ray, A. S. Nowick, J. Solid State Chem. 1975, **15**, 344-351.
23 I. Riess, 1985, **57**, 314-322.
24 M. Yashima, S. Kobayashi, T. Yasui, Solid State Ionics 2006, **177**, 211-215.
25 M. Yashima, D. Ishimura, Y. Yamaguchi, K. Ohoyama, K. Kawachi, Chem. Phys. Lett. 2003, **372**, 784-787.
26 S. Hull, S. T. Norberg, I. Ahmed, S. G. Eriksson, D. Marrocchelli, P. A. Madden, J. Solid State Chem. 2009, **182**, 2815 – 2821.
27 E. A. Kummerle, G. Heger, J. Solid State Chem. 1999, **147**, 485-500.
28 C. W. Sun, H. Li, Z. X. Wang, L. Q. Chen and X. J. Huang, Chem. Lett. 2004, 662–663.
29 G. S. Wu, T. Xie, X. Y. Yuan, B. C. Cheng and L. D. Zhang, Mater. Res. Bull. 2004, **39**, 1023–1028.
30 Z. Y. Sun, H. Y. Zhang, G. M. An, G. Y. Yangand, Z. M. Liu, J. Mater. Chem. 2010, **20**, 1947–1952.
31 W. Q. Han, L. J. Wu and Y. M. Zhu, J. Am. Chem. Soc. 2005, **127**, 12814–12815.
32 C. C. Tang, Y. Bando, B. D. Liu and D. Golberg, Adv. Mater. 2005, **17**, 3005–3009.
33 Z. Tang, Y. Zhang and Y. Xu, RSC Adv. 2011, **1**, 1772–1777.
34 Wei, J. Liu, Z. Zhao, A. J. Duan, G. Y. Jiang, C. M. Xu, J. S. Gao, H. He and X. P. Wang, Energy Environ. Sci. 2011, **4**, 2959–2970.
35 S. Chunwen, L. Hong, Ch. Liquan, Energy Environ. Sci. 2012, **5**, 8475-8505.
36 G. S. Herman, Surf. Sci. 1999, **437**, 207–214.
37 J. C. Conesa, Surf. Sci. 1995, **339**, 337–352.
38 E. Mamontov, T. Egami, R. Brezay, M. Koranne and S. Tyagi, J. Phys. Chem. B 2000, **104**, 11110–11116.
39 P. Gao, Z. Kang, W. Fu, W. Wang and X. Bai, J. Am. Chem. Soc. 2010, **132**, 4197–4201.
40 B. W. Sheldon and V. B. Shenoy, Phys. Rev. Lett. 2011, **106**, 216104.
41 M. Shelef, Catal. Today 2000, **62**, 35-50.
42 M. Twigg, Appl. Catal. B 2007, **70**, 2-15.
43 H. P. Bonzel, R. Ku, Surf. Sci. 1972, **33**, 91-106.
44 G. Ertl, Surf. Sci. 1994, **299-300**, 742-754.
45 P. Mars, D. W. van Krevelen, Spec. Suppl. Chem. Eng. Sci. 1954, **3**, 41–57.
46 H.Y. Kim, H. M. Lee, G. Henkelman, J. Am. Chem. Soc. 2012, **134**, 1560-1570.
47 P. Bera, A. Gayen, M.S. Hegde, N. P. Lalla, L. Spadaro, F. Frusteri, F. Arena, J. Phys. Chem. B 2003, **107**, 6122-6130.
48 K. R. Priolkar, P. Bera, P. R. Sarode, M. S. Hegde, S. Emura, R. Kumashiro, N. P. Lalla, Chem. Mater. 2002, **14**, 2120-2124.
49 M. S. Hegde, G. Madras, K. C. Pail, Acc. Chem. Res. 2009, **42**, 704-712.
50 B. Penkala, W. Paulus, H. Kaper, EMRS Fall Meeting, Warsaw 2014, pp. 347.
51 K. Gupta, S. Singh, M. Ceretti, M. S. Ramachandra Rao, W. Paulus, Phys. Status Solidi A, 2013, 1-7.
52 Z. V. Popovic, Z. Dohcevic-Mitrovic, A. Cros and A. Cantarero, J. Phys. Condens. Matter. 2007, **19**, 496209-496218.
53 Z. Dohcevic-Mitrovic, Z. V. Popovic, M. Scepanovic, Acta Phys. Pol. A 2009, **116**, 1, 36-41.
54 T. X. T. Sayle, S. C. Parker, C. R. A. Catlow, Surf. Sci. 1994, **316**, 329-336.
55 U. Hennings, R. Reimert, Appl. Catal. A-Gen. 2007, **325**, 41-49.
56 G. N. Vayssilov, Y. Lykhach, A. Migani, T. Staudt, G. P. Petrova, N. Tsud, T. Skala, A. Bruix, F. Illas, K. C. Prince, V. Matolin, K. M. Neyman, J. Libuda, Nat. Mater. 2011, **10**, 310-315.
57 H.-H. Liu, Y. Wang, A.-P. Jia, S.-Y. Wang, M.-F. Luo, J.-Q. Lu, Appl. Surf. Sci., 2014, **314**, 725-734.

Catalysis Science & Technology

ARTICLE

Role of Lattice Oxygen on CO Oxidation Over $Ce^{18}O_2$-Based Catalyst Revealed Under Operando Conditions.

Bartosz Penkala [a b], Daniel Aubert[b], Helena Kaper[b], Caroline Tardivat[b], Kazimierz Conder[c] and Werner Paulus[a].

Graphical Abstract

Understanding role of lattice oxygen on CO oxidation over ceria based compounds, revealed by combination of novel isotope-based techniques, namely temperature-controlled Isotope LAbeling Raman Spectroscopy (ILARS) and Isotope Labeling Pulse Temperature Programed Oxidation Reaction (ILPOR).